Lithium Adsorption on Graphite from Density Functional Theory Calculations

ARTICLE *in* THE JOURNAL OF PHYSICAL CHEMISTRY B · SEPTEMBER 2006

Impact Factor: 3.3 · DOI: 10.1021/jp062126+ · Source: PubMed

4 AUTHORS:

Felipe Valencia
National University of Colombia
14 PUBLICATIONS **157** CITATIONS
SEE PROFILE

A.H. Romero
West Virginia University
253 PUBLICATIONS **3,513** CITATIONS
SEE PROFILE

F. Ancilotto
University of Padova
152 PUBLICATIONS **2,435** CITATIONS
SEE PROFILE

Pier Luigi Silvestrelli
University of Padova
93 PUBLICATIONS **3,289** CITATIONS
SEE PROFILE

Lithium Adsorption on Graphite from Density Functional Theory Calculations

Felipe Valencia*

Dipartimento di Fisica Galileo Galilei, Universitá degli Studi di Padova, Via F. Marzolo, 8-35131 Padova, Italy

Aldo H. Romero

CINVESTAV-QUERETARO, Libramiento Norponiente No. 2000 Real de Juriquilla 76230, Queretaro, Qro, Mexico

Francesco Ancilotto and Pier Luigi Silvestrelli

Dipartimento di Fisica Galileo Galilei, Universitá degli Studi di Padova, and DEMOCRITOS National Simulation Center, Trieste, Italy

Received: April 5, 2006; In Final Form: June 12, 2006

The structural, energetic, and electronic properties of the Li/graphite system are studied through density functional theory (DFT) calculations using both the local spin density approximation (LSDA), and the gradient-corrected Perdew−Burke−Ernzerhof (PBE) approximation to the exchange-correlation energy. The calculations were performed using plane waves basis, and the electron−core interactions are described using pseudopotentials. We consider a disperse phase of the adsorbate comprising one Li atom for each 16 graphite surface cells, in a slab geometry. The close contact between the Li nucleus and the graphene plane results in a relatively large binding energy (larger than 1.1 eV). A detailed analysis of the electronic charge distribution, density difference distribution, and band structures indicates that one valence electron is entirely transferred from the atom to the surface, which gives rise to a strong interaction between the resulting lithium ion and the cloud of π electrons in the substrate. We show that it is possible to explain the differences in the binding of Li, Na, and K adatoms on graphite considering the properties of the corresponding cation/aromatic complexes.

1. Introduction

The interest in the interaction between a lithium atom and a graphite substrate feeds from at least two related sources. First, diffusion on—and into—the graphite surface precedes the formation of lithium−graphite intercalation compounds (Li−GICs).[1,2] Li−GICs have been actively investigated ever since the early 1980s,[3−5] with a major boost after the realization of the first rechargeable Li-ion batteries, achieved thanks to the replacement of lithium metal electrodes by lithium intercalated carbon hosts.[6,7] Second, the Li on graphite system falls under the scope of a broader field of research, concerning the adsorption of alkali metals on graphite substrates. This latter idea has also been an active field during the past two decades.[1,2,8−26] Catalysis of gasification reactions,[21,23] and hydrogen physisorption[27] in graphitic hosts, might be improved by alkali adatoms. One of the most relevant issues in the field is the nature itself of the adsorbate−substrate bonding. That question was posed at a very early stage of this research, and many experimental and theoretical efforts have been concerned with gathering the evidence required to answer it. Examinations performed at monolayer and submonolayer coverages are particularly relevant in that respect.[2,10,13,14,19,25]

The experimental[2,10,13,17,19,20,23,25,28] and theoretical[11,12,15,22,29] evidence summoned through the years consistently signals that alkali atoms are adsorbed preferentially on top of *hollow* sites, that is, above the center of a hexagon in the graphene layer immediately below. At low coverages, the distance between neighboring adatoms has been found to be quite large (for instance, up to 60 Å in K/graphite), evidencing a strong repulsive interaction.[8] A significant amount of charge is transferred from the alkali metal to the carbon substrate in these dispersed phases.[8] When the coverage is increased, the interaction between the alkali metals grows in importance and the charge transfer to the substrate decreases. Above a certain limit for the density of adatoms, nucleation into solid islands on the surface can be observed.[2,8,13,16,19]

Those investigations have focused mainly on the properties of potassium adatoms, also because of the relative ease with which layer-by-layer growth has been achieved.[8,10,14] Due to the similarities between the members of the alkali family, many of the conclusions drawn for the binding mechanism in K/graphite might be expected to hold true for other alkali metals. The small atomic radius of lithium, however, is known to lead to significant differences between Li−GICs and other alkali−GICs.[3,5] Similar differences might be expected for the adsorbed species. Most of the information regarding the Li/graphite binding comes from theoretical calculations[11,27,30−34] which, however, happen to be relatively scarce and not yet definitive. The reported binding energies range from about 0.65 eV[30,34] to about 1.7 eV,[11,31] while the calculated distance to the graphite surface varies from 1.64[11] to 2.1 Å[31] and even to 3.3 Å in the molecular-mechanics approach of ref 32. Apart from these molecular-mechanics calculations, which favor adsorption on

* To whom correspondence should be addressed. Fax +39-049-8277102. Tel: +39-049-8277251. E-mail: felipevh@pd.infn.it.

10.1021/jp062126+ CCC: $33.50
Published on Web 07/13/2006

TABLE 1: Lattice Parameters, Bulk Modulus (B_o), and C_{33} Elastic Constants Calculated for Graphite Using Different *k*-point Meshes[a,b]

	16 × 16 × 4 mesh	12 × 12 × 2 mesh	8 × 8 × 2 mesh	
		a_0 (Å)		
LSDA	2.462	2.462	2.460	
PBE	2.469	2.469	2.469	
expt				2.460[c]
		c_0/a_0		
LSDA	2.680	2.670	2.662	
expt				2.726[c]
		E_{cohe} (eV/atom)[d]		
LSDA	8.828	8.825	8.28	
PBE	7.776	7.774	7.776	
expt				7.37[d]
		B_o (GPa)		
LSDA	42	46	53	
expt				34−42[e]
		C_{33} (GPa)		
LSDA	51	49	32	
expt				36[f]

[a] Experimental values are also reported for comparison. [b] The reported values were obtained using a cutoff of 38 Ry. [c] Reference 50 and references therein. [d] The reference for the cohesive energies is the calculated energy for the isolated C atom in the triplet state. [e] Reference 66 and references therein. [f] Reference 51 and references therein.

the top site,[32] the *hollow* site is consistently identified as the preferential adsorption site. Each one of the ab initio calculations we are aware of[11,27,33,34] uses a different approach to the problem, thus making a meaningful comparison difficult. Constance and Rao[33] used a generalized-gradient approximation (GGA) approach to the density functional theory (DFT) in a small cluster model of two graphene layers; Kantha et al.[11] used the LDA approximation in a slab geometry for graphene; Zhu and Lu[34] applied both the MP2 perturbation theory and a GGA approximation to cluster graphene models with different sizes (between 7 and 14 hexagonal rings); Cabria et al.[27] used both LDA and GGA approximations in graphene models with the slab geometry. Recently, the adsorption of lithium on novel carbon allotropes (especially nanotubes) has also been addressed.[30,31,35−37] The proper rationalization of the effects observed in these studies requires a more accurate quantification of the binding energy on simple graphite.

In this paper, we address the binding mechanism between a lithium adsorbate and the graphite surface. Our study is based on DFT calculations, using a supercell geometry. We examine the effects of the different parameters characterizing our computational model, in particular, the number of graphene layers, the accuracy of the *k*-point sampling of the Brillouin's zone, and the type of exchange-correlation energy functional used. Our results allowed us to draw a relatively simple picture of the binding mechanism and give estimations for the binding energies. Moreover, the comparison with the corresponding calculated properties for Na and K adatoms allows for a critical revision of previous statements concerning the ordering of the binding energy on these three adsorption systems.[29,34]

2. Computational Methods

The reported results were obtained in the framework of the DFT using both the local spin density approximation (LSDA) in the Perdew−Zunger parametrization[38] and the generalized-gradient-corrected Perdew−Burke−Ernzerhof (PBE) approximation[39] to the exchange-correlation potential. The Kohn−Sham orbitals were expanded using plane waves, and the interaction between the valence electrons and the ionic core was described using pseudopotentials.

For the LSDA calculations, we used norm-conserving pseudopotentials of the Von Barth−Car form,[40] considering four valence electrons for carbon and one for the alkali species. The pseudopotentials for the alkali atoms included nonlinear core corrections.[41] The pseudopotentials adopted for C and Na were already used in ref 42; the one used for K was instead taken from ref 22. In these and other works,[43,44] they were found to provide reliable descriptions of the chemical interaction between sp^2 hybridized carbon structures and the corresponding alkali metals.

In the case of PBE calculations, we used ultrasoft (Vanderbilt) pseudopotentials,[45] with four valence electrons for carbon, three for lithium and nine for sodium and potassium.[46] These pseudopotentials provided good results for the bulk structures. To test their reliability for the graphite−alkali chemical environment we also checked the results for $A-C_6H_6$ (A = Li, Na, K) molecules, as will be discussed in the following.

All the calculations were performed using the Quantum-ESPRESSO ab initio package.[47]

In Table 1, we report the structural and electronic properties calculated for crystalline graphite. The practical implementations of the DFT lack a proper description of the dispersive forces between graphene layers; however, this flaw is partially compensated by the overbinding character of the LSDA.[48−52] Taking this fact into consideration, for the LSDA calculations, we searched for the minimum energy configuration varying both the in-plane, a_0, and out-of-plane, c_0, lattice parameters. The Bulk modulus, B_0, was obtained by fitting the energy vs volume curves to the Birch−Murnaghan formula,[53] and the C_{33} elastic constant was obtained by a polynomial fit of the total energy vs c_0 curve at the optimal a_0 value. PBE, like other GGA approximations, does not provide a proper binding among the graphene layers. Therefore, in that case, we searched only for the optimized a_0 parameter, with the c_0 parameter set to its experimental value.

According to our tests, the structural and energetic properties are well converged using a 38 Ry cutoff and 90 special *k*-points (the 16 × 16 × 4 Monkhorst-Pack mesh). The band structures depicted in Figure 1 are in quite good agreement with results from all-electron calculations.[51] Besides, LDA and PBE yield mostly the same dispersion curves.

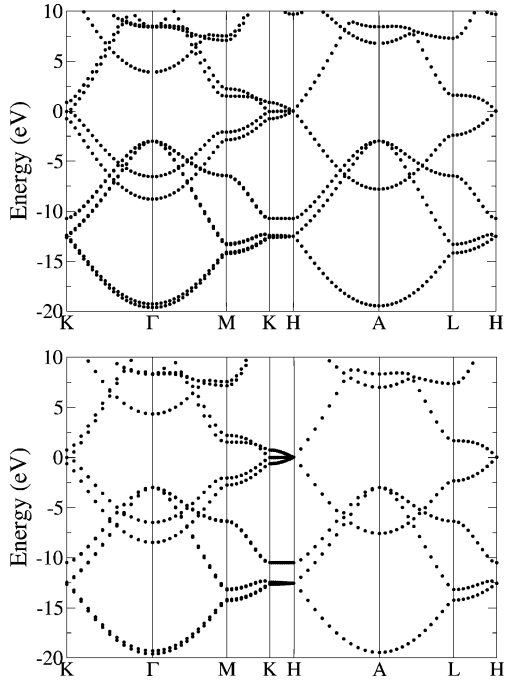

Figure 1. Electronic band dispersion curves calculated for graphite, using the LSDA approximation (top) and the PBE approximation (bottom). The zero of the energy axis corresponds to the Fermi level.

TABLE 2: Structural Parameters and Cohesive Energies for the Graphite Surface Models Used in This Work[a]

	$a_0/4$ (Å)	d_0 (Å)[b,c]	E_{cohe}(eV/atom)
		C32[d]	
LSDA	2.461		8.794
PBE	2.470		7.794
		C64[e]	
LSDA	2.461	3.273	8.814
PBE	2.470	3.348[f]	7.784
		C96[g]	
LSDA	2.461	3.280	8.818
PBE	2.470	3.348[a]	7.780

[a] The reported values were obtained using a cutoff of 38 Ry for the plane-waves kinetic energy and nine special *k*-points. [b] a_0 is the supercell in-plane lattice parameter. [c] Distance between consecutive graphene layers. [d] Single graphene layer with 32 atoms (4×4 cells of graphene). [e] Model with two graphene layers. [f] Fixed to the experimental value. [g] Model with three graphene layers.

We performed our calculations using supercell models with one (C_{32}), two (C_{64}), and three (C_{96}) graphene layers, each one with 32 carbon atoms, stacked in the Bernal structure. The distance to the periodic images in the direction normal to the surfaces was at least 18 Å. The geometries of these models for the substrate were optimized with respect to the in-plane lattice parameter, a_0. For the LSDA calculations, we scanned different values of the interlayer separation, d_0, whereas for PBE, the interlayer distance was fixed to the experimental bulk value. In these steps, we always used the same 38 Ry cutoff. The use of nine *k*-points (a $5 \times 5 \times 1$ Monkhorst-Pack mesh) was found necessary to obtain well-converged values. The resulting structural and energetic parameters are reported in Table 2.

The electronic dispersion curves for models with more than one layer (see Figure 2) resemble more closely that for the graphite crystal. This improvement in the description of the electronic structure of the substrate might be relevant in the characterization of the alkali−graphite adsorption processes; this fact has already been acknowledged in the literature,[9,54] and that we will recall in the following.

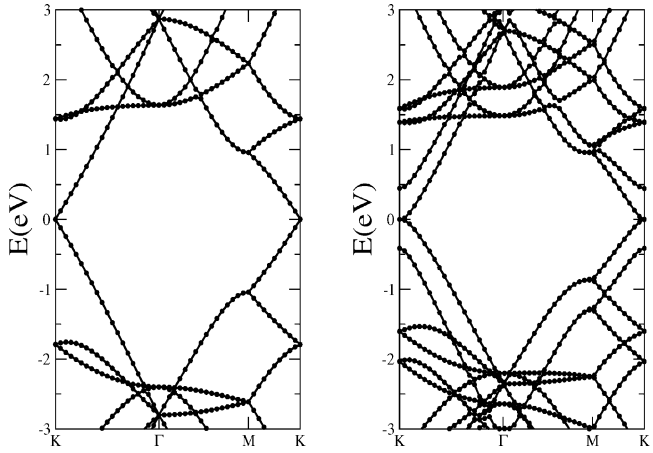

Figure 2. Electronic bands dispersion curves for the C_{32} (left panel) and C_{64} (right panel) slab models. We show the results for LSDA calculations; PBE yields very similar dispersion curves.

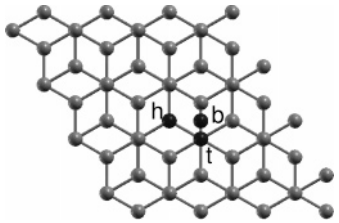

Figure 3. Hollow (h), top (t), and bridge (b), adsorption sites on the graphite surface; darker spheres represent the alkali adatoms.

We considered a single adsorbate on each one of the slab surfaces, corresponding to relatively disperse adsorption phases (the distances between neighboring alkali atoms being about 9.8 Å). Although these model superstructures do not correspond to experimentally observed phases,[8] they can be expected to serve our purpose of analyzing the bond properties in the disperse phases.

The adatoms were originally set to lie on top of the hollow (h), top (t), and bridge (b) positions of the graphite surface (see Figure 3), at distances estimated from the previously reported values. The Broyden−Fletcher−Goldfarb−Shanno (BFGS) algorithm[55] was then used to obtain the optimized geometries. In the LSDA calculations, both the alkali and carbon atoms coordinates were optimized. For the PBE cases, we relaxed only coordinates of the alkali atom and of its neighboring C atoms. We obtained well-converged structural parameters using nine special *k*-points and kinetic energy cutoffs of 38 Ry (for LSDA) and 68 Ry (for PBE). The electronic properties and binding energies were calculated using larger cutoffs of 48 and 80 Ry, respectively. This choice of parameters lead to total energies converged below 2 meV in terms of the *k*-points sampling and kinetic energy cutoff.

To study the band dispersion curves, we used the self-consistent charge densities obtained using nine special *k*-points, in non-self-consistent calculations along high symmetry points of the Brillouin zone. A similar procedure allowed us to obtain well-converged electronic densities of states and densities of states projected on localized orbitals.

For the analysis of the charge-transfer processes, we used four different approaches: (i) the study of the density difference (*bond density*) distribution induced by the bond's formation,[57] (ii) the Bader's atoms in molecules theory,[56] (iii) the analysis of the charge contained in Voronoy's polyhedra centered at the adatoms,[58] and (iv) the Löwdin analysis obtained from the projected electron densities of states. The Löwdin analysis has

TABLE 3: Binding Distances, $d_\perp$,[a] and Binding Energies, E_b, Calculated for Lithium Adatoms[b]

			$d_\perp$ (Å)	E_b (eV)
C_{32}	LSDA	Γ-point	1.64	0.76
	LSDA	*k*-points	1.63	1.55
	PBE	Γ-point	1.75	0.17
	PBE	*k*-points	1.67	1.01
C_{64}	LSDA	*k*-points	1.63	1.68
	PBE	*k*-points	1.71	1.10
C_{96}	LSDA	*k*-points	1.63	1.68
Cabria et al.[27]	LDA	*k*-points	1.80	0.75
	PW91	*k*-points	1.86	0.43
Zhu and Lu[34]	B3LYP	cluster[c]	1.74	0.64
	B3LYP	cluster[d]	1.71	1.36
	MP2	cluster[c]	2.09	0.98
Constance et al.[33]	BPW91	cluster[d]	1.76	1.38
Khantha et al.[11]	LDA	*k*-points	1.64	1.60
Dubot et al.[31]	NDDO		2.10	1.70

[a] Average perpendicular distance to the carbon atoms in the first graphene layer. [b] Values estimated by other authors are also reported. Here we included only a citation of the method used in each case, details can be found in the corresponding references. In our calculations, *k*-points indicate a nine *k*-points sampling of the Brillouin zone. [c] Adsorption on a hydrocarbon model with a closed-shell electronic state. [d] Adsorption on a hydrocarbon model with an open-shell electronic state.

a large extent of arbitrariness due to the selection of the atomic-like projections, and this kind of analysis is included mostly for the sake of completeness.

3. Structural and Electronic Properties of Lithium Adsorbed on Graphite

In accordance with the established scenario, our calculations predict that lithium adatoms adsorb preferentially on hollow sites. The bridge and top sites are energetically less favored by 0.34 and 0.36 eV, respectively. Therefore, we mainly focus on elucidating the binding mechanism at the most stable (hollow) site. The data reported in Table 3 summarizes the results of our geometrical optimizations for lithium adatoms. The substrate geometry was slightly modified by the bond formation. In particular, the carbon atoms in the hexagonal ring lying just below the adatom are pushed downward by about 0.015 Å. We explicitly considered spin polarization, and the magnetic moment of the supercell

$$M = \int_{\text{cell}} [\rho^{\text{up}}(r) - \rho^{\text{down}}(r)]\, \mathrm{d}^3 r$$

was also optimized in the calculations. The studied models comprise an odd number of electrons. For the calculations using only the Γ-point to sample the Brillouin zone, we found significant gaps between the LUMO and LUMO-1 levels (~3.5 eV). This fact is related to the large HOMO−LUMO gaps for the graphite substrate models when only the Γ-point is considered. Because of this discretization of the available electronic states, the only possibility is to have that the total magnetization of the system is $M = 1\ \mu_B$. Through the use of additional *k*-points, it was possible to approach the metallic density of states of the system and we obtained nonmagnetized supercells.

The calculated stable geometries are mostly independent of the use of different *k*-point samplings and of the number or layers considered for the substrate. The binding energies, however, increased by about 0.1 eV when two layers were considered. The inclusion of a third layer using the LSDA functional did not result in significant changes, and the same trend might be expected for the PBE calculations. Both in the LDA and PBE frameworks, Γ-point-only calculations underestimate the binding energy by about 0.8 eV, when compared with calculations using additional *k*-points.

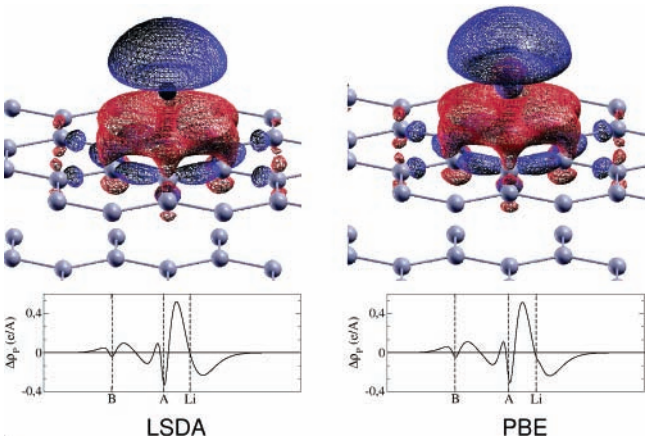

Figure 4. Top: two isosurfaces of the density difference distribution, $\Delta\rho = \rho[\mathrm{LiC_{64}}] - \rho[\mathrm{C_{64}}] - \rho[\mathrm{Li}]$, calculated for the Li/graphite system; red surfaces correspond to charge gains of 0.015 e/Å^3 and blue surfaces are for an equivalent charge lost. Bottom: the density difference integrated over planes lying parallel to the graphite's surface, $\Delta\rho_P = \int_{x,y} \Delta\rho\, \mathrm{d}A_\perp$. Results for both the LDA and PBE calculations are shown.

We also calculated the binding energy in the LiC_6H_6 molecule, an alkali−aromatic complex that has been studied by means of very accurate quantum mechanical calculations.[59] The reported value for the distance between the Li atom and the center of the benzene ring is 2.25 Å, with a binding energy of about 0.33 eV. Our LSDA calculations yielded 1.65 Å and 0.71 eV, displaying a clear overbinding character. The PBE calculations performed better (1.90 Å and 0.21 eV). Despite the similar local chemical environment, the binding mechanisms for Li−graphite and Li−benzene are different. As discussed in ref 59, electron correlation effects and dispersion interactions contribute to the Li−benzene binding. Contributions from dispersive terms in the Li−graphite adsorption were discussed by Kantha et al.[11] The significant charge transfer between Li and the graphite substrate, however, provides for stronger interactions. In Figure 4, we display the charge density difference

$$\Delta\rho = \rho[\text{Li} - \text{substrate}] - \rho[\text{Li}] - \rho[\text{substrate}] \qquad (1)$$

between the charge densities of the adsorption system and those of the separated substrate and adatom (at the optimized positions). The most evident difference between the LSDA and PBE results in Figure 4 is the slight polarization in the core region of the Li atom observed in the PBE calculation. As mentioned in section 2, the pseudopotentials for LSDA consider only one valence electron, therefore this polarization cannot be expected to appear in the LSDA. However, the main features turn out to be the same in both approaches. Charge in the nonbonded region of the lithium atom migrates to the bonding region. Also, the charge in the C−C bonds decreases, especially for those nearest to the Li atom. The shape of the charge density difference in the bonding region suggests an increased population of p_z-like graphite orbitals; these are subsequently either deformed by the interaction with the positive charge in the lithium atom or hybridized with localized adatom states. We found that the position and width of the charge-gain hump right after the underlying graphene layer (see the bottom part of Figure 4) do not vary when we considered Na and K adatoms, thus indicating that this feature is actually dominated by the electronic states of the substrate. Notice that the position of the Li ion coincides almost exactly (exactly in the LSDA case) with

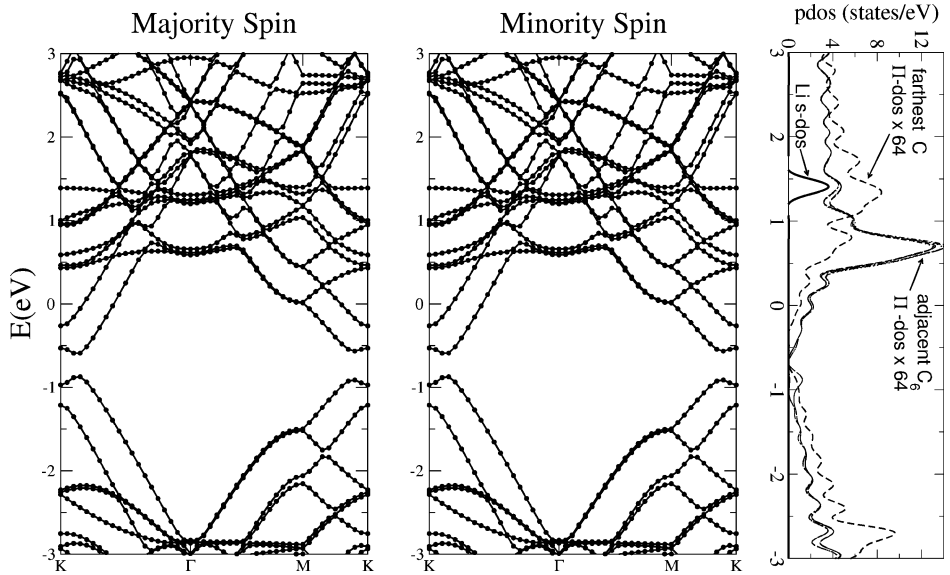

Figure 5. Electronic band dispersion curves for Li adsorbed on the C_{64} slab model, using the LSDA approach. The zero of the energy axis corresponds to the Fermi level. The last panel to the right shows the *p*-like projected density of electronic states for the hexagonal ring closest to the adsorbed atom and the most distant C atom. The *s*-like projected density of states for Li is also shown.

the point at which this hump crosses the zero transfer axis. Therefore, it is possible to state that the electronic density of the graphite cloud of the Π-electron is significant in the close neighborhood of the Li atom. The binding distance to the substrate roughly corresponds to the expected value in the van der Waals spheres model of the system. These two characteristics correspond to the scenario referred to as *bare*, or *van der Waals*, contact among chemical species.[61]

Alkali cations in bare contact with aromatic rings display a relatively strong noncovalent bond, referred to as the cation−Π interaction.[61] In the case of Li^+, the induction interaction—the deformation of the aromatic ring's charge density—contributes strongly to the bond.[63] High-level quantum mechanical calculations determined that the binding energies increase with the number of aromatic rings, going from ∼1.58 eV (for $Li^+-C_6H_6$) to ∼2.12 eV (for $Li^+-C_{54}H_{18}$).[64] The charge distribution we found for Li−graphite suggests that a similar mechanism might be responsible for the bond. If we assume that nearly one electron is transferred from the Li atom to the graphite surface, a rough estimation of the binding energy could be achieved from those values. If we take the $Li^+-C_{54}H_{18}$ model as roughly describing the electrostatic and induction interactions between the Li atom and the substrate, the binding energy would be approximately given by this binding energy minus the energetic cost of the charge transfer, that is

$$E_b \sim 2.12\ \text{eV} - (\text{IP[Li]} - W_f\text{[Graphite]}) = 1.32\ \text{eV} \qquad (2)$$

where IP and W_f are the ionization potential and work function, respectively. This crude estimation is consistent with our DFT results. It would also help to understand the significant difference between the Γ-point and *k*-points results. For Γ-point calculations, the first empty state in the substrate is far above the Fermi level, increasing significantly the cost associated with the charge transfer (see Figure 2). The differences in the binding energies calculated using cluster models with open- or closed-shell electronic states[34] seem to follow a similar rationale.

We now turn to the description, and quantification, of the charge transferred from Li to the graphite surface. First, we examined the electronic dispersion curves and the electronic densities of states projected on localized orbitals (see Figure 5). It is remarkable that the model comprising a single graphene layer does not display the gap opening in the valence region, a feature that has already been discussed in the literature.[9] The position of the *s*-like lithium electronic states, high above the Fermi level, supports the idea of a large charge transfer. Besides, we did not found additional flat states in the valence region, which should correspond to occupied states localized at the lithium atom. The local density of *p*-like states near the Fermi level is increased for the hexagonal carbon ring below the alkali metal, which is consistent with the charge density differences. The Löwdin analysis gives a value for the charge transfer of ∼0.60 e; the electronic density attached to the Li atom was found at *p*-like localized wave functions. For the sake of comparison, the Mulliken charge analysis of ref 34 estimated the charge transfer to be 0.43 e.

Löwdin and Mulliken analysis are quite sensitive to calculation details. In particular, the type of projectors used for the Löwdin analysis might influence the quantification of the charge transfer. This fact could be expected to affect particularly when, as in the studied case, the different considered species are at van der Waals contact. Further, the shape of the density change clouds does not support the picture of $p-\sigma$ hybridization between the graphite p_z states and the *p* Li states indicated by the Löwdin analysis. From a quantum mechanical point of view, a measure of the electronic charge distribution can be achieved by analyzing the topology of the electronic density. The gradient of the charge density must vanish in the direction normal to the boundaries defining atomic regions.[56] Once these atomic regions are determined, it is straightforward to define the atomic charges. We applied the Bader analysis to the generated charge densities,[60] obtaining values of 1.0 and 0.89 e for the charge transfer (LSDA and PBE calculations respectively). We did not correct the charge densities in the core regions, a condition which might affect the obtained values. It must be recalled that the LSDA pseudopotentials considered only one valence electron for Li, whereas PBE pseudopotentials considered also the core−shell electrons. The relatively good agreement between the values obtained by these two approaches suggests that our estimations are accurate enough. The neighborhood of the Li atom is not devoid of charge in the LSDA calculations. The electronic charge density calculated in the LSDA framework

showed a rather delocalized profile in the neighborhood of the Li atom, suggesting again that the contribution of lithium atomic-like states to the density is actually very small.

We further analyzed the planar integrated density difference profiles in Figure 4. In particular, we considered the charge lost in the nonbonded region

$$\Delta c_{nb} = \int_{z(Li)} \Delta\rho_P \, dz \quad (3)$$

where z(Li) is the z-position of the Li atom and the charge lost in the negative peaks near the alkali adatom[22]

$$\Delta c_1 = \int_{z(X)} \Delta\rho_P \, dz \quad (4)$$

where z(X) stands for crossing point between the jump near the graphite surface and the zero transfer axis. The two definitions are thus equivalent in the LSDA case. The calculated values displayed a systematic dependence with the size of the supercell in the normal direction, c_0, this fact is related to the induced electric dipole at the alkali−graphite interface. In the LSDA calculations, we followed this dependency up to $c_0 \sim 30$ Å. The functional dependence could be fitted to a law

$$\Delta c + \text{constant}/c_0^3$$

The $1/c_0^3$ contribution was very small, and the value calculated with $c_0 = 23.5$ Å was only ∼1% higher than the extrapolated value of $\Delta c_1 = \Delta c_{nb} = 0.380$ e. We did not attempt to assess this functional dependence in the PBE calculations, because of the higher computational cost. The corresponding PBE values using $c_0 = 23.5$ Å were $\Delta c_1 = 0.390$ e and $\Delta c_{nb} = 0.380$ e. These quantities measure the amount of electronic charge transferred to the bond region. Another useful description of the density redistribution could be achieved by considering the change in the total charge contained in a Voronoy polyhedra centered at the adatom position. This quantity is usually referred as the Voronoy deformation density,[58] VDD. We estimated this value to be VDD = 0.42 e, in LSDA, and VDD = 0.47 e, the PBE result. These relatively low estimations of the charge transfer, and the accumulation of charge in the bonding region, could be interpreted as hints of a partially covalent share of the charge between the substrate and the alkali atom. As mentioned above, the charge density profiles do not support the idea of hybridization among the atomic and substrate orbitals. The contrast between the charge-transfer estimations based on simple geometric partitions, and the values obtained by Bader's analysis, is related to the different features targeted by each one of these tools. Bader's charges and electronic band structure analysis attempt a proper quantum mechanical partition of the electronic density. They suggest that most of the charge density in the bonding region corresponds to electrons occupying electronic states of the substrate, rather than covalently shared with the alkali atom. Moreover, we searched for the maximally localized Wannier functions.[62] The Wannier function center corresponding to the valence electron of the Li atom was found to be associated with π bonds in the underlying hexagonal ring. On the other hand, VDD, Δc_1, and Δc_{nbb} address the classical aspects of the charge distribution. Therefore, their values should be related to the screening of the core's charge by the electronic cloud, which is expected to be significant due to the delocalization of the substrate's electrons in the adatom's surroundings.

The charge density difference profiles, electronic dispersion curves, and Bader analysis consistently indicate a large (∼1 e) charge transfer from the lithium atom to the graphite substrate. In that scenario, a significant contribution to the interaction energy can be expected to arise from the attraction between the π-electrons cloud of graphite and the ionized atom. The shape of the density difference clouds supports this interpretation. In their study of the dependence of the binding energy with distance, Khantha et al.[11] found a strong $1/d^4$ contribution, which might arise from the dependence of the induction energy in cation−π complexes.[63]

The charge distribution gives rise to a relatively large electric dipole moment in the z direction. The above-mentioned dependency of the charge distribution on the vacuum region affects the evaluation of this dipole moment, which was found to display the same $D + A/x^3$ trend. From the LDA calculations using different c_0 parameters, we found a value of 4.97 D for $c_0 = 23.5$ Å and an extrapolated value of 4.47 D. The PBE calculation at $c_0 = 23.5$ Å yielded 5.40 D.

As discussed by Cabria et al.,[27] the binding energy of an isolated Li atom must be expected to be larger than the values found in supercell calculations, due to the long-range Coulombic interaction between the Li adatoms in these latter cases.

TABLE 4: Binding Distances ($d_\perp$), Binding Energies (E_B), and Supercell Magnetization ($|M|$),[a] for Li, Na, and K Adsorbed on Graphite[b]

	$d_\perp$ (Å)	E_B (eV)	$\lvert M\rvert(\mu_B)$
	Li		
LSDA[c]	1.63	1.68	0.00
PBE[c]	1.71	1.10	0.00
	Na		
LSDA[c]	2.42	0.69	0.28
PBE[c]	2.34	0.50	0.27
PBE[d]	2.45	0.51	
B3LYP[e]	2.09	−0.002	
B3LYP[f]	2.10	0.71	
	K		
LSDA*c*	2.70	1.12	0.17
PBE[c]	2.65	0.88	0.18
LDA[g]	2.76	0.78	
LDA[h]	2.79	0.51	
B3LYP[e]	2.54	0.35	
B3LYP[f]	2.51	1.06	
LSDA[i]	2.73	1.65	
GGA[i]	2.81	1.44	
expt[j]	2.79 ± 0.03		

[a] The magnetization is calculated by the integration of the difference between the spin up and spin down electronic densities: $M = \int \{\rho^{up}(\vec{r}) - \rho^{down}(\vec{r})\} \, d\vec{r}$. [b] For details, please refer to the original references. Some other theoretical and experimental values are reported for comparison. [c] This work, using the C_{64} model. [d] Slab calculation, from ref 12. [e] Cluster model with a close-shell electronic state, from ref 34. [f] Cluster model with an open-shell electronic state, from ref 34. [g] Slab calculation, ref 22. [h] Slab calculation, ref 54. [i] Cluster model, ref 15. [j] LEED study for the 2 × 2 structure, ref 10.

4. Comparison with Sodium and Potassium Adatoms on Graphite

In Table 4, we compare the structural properties calculated for lithium, sodium, and potassium adsorbed on the hollow site (which was found to be the preferred site in each case) of graphite. The binding distances to the graphite substrate correspond roughly to the van der Waals contact distances and, thus, to the bond lengths in related cation−π complexes (1.87, 2.42, and 2.80 Å for Li^+, Na^+, and K^+ on benzene, respectively[63]). When compared at the same theory levels, the binding energies are ordered in a sequence that does not correspond either to a purely electrostatic trend (Li > Na > K) or to the ordering in the ionization potentials (K > Na > Li). This fact has already been pointed out in refs 34 and 29.

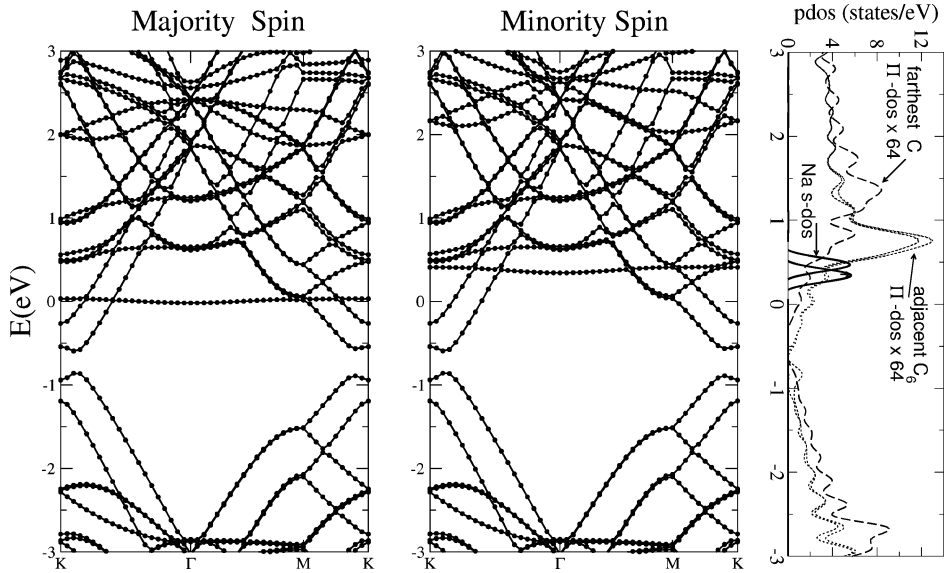

Figure 6. Electronic band dispersion curves for Na adsorbed on the C_{64} slab model. The zero of the energy axis corresponds to the Fermi level. The last panel to the right shows the *p*-like projected density of electronic states for the hexagonal ring closest to the adsorbed atom and the most distant C atom. The *s*-like projected density of states for Na is also shown.

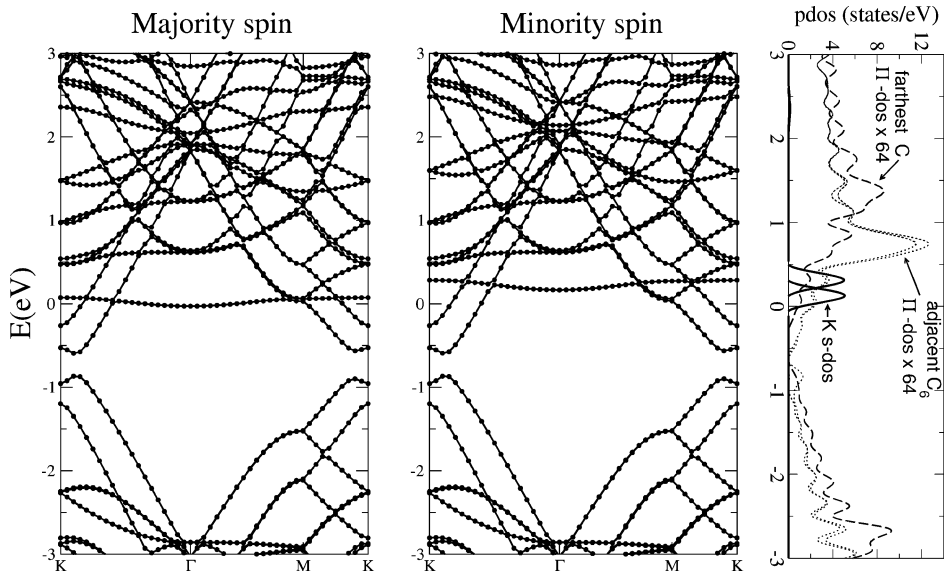

Figure 7. Electronic band dispersion curves for K adsorbed on the C_{64} slab model. The zero of the energy axis corresponds to the Fermi level. The last panel to the right shows the *p*-like projected density of electronic states for the hexagonal ring closest to the adsorbed atom and the most distant C atom. The *s*-like projected density of states for K is also shown.

We explicitly considered spin magnetization, and the corresponding magnetic moments in the supercells are also reported in Table 4. The differences between the spin-polarized and non-spin-polarized energies were, however, very small: 8 meV for K and 0.19 meV for Na. To the best of our knowledge, there is no evidence of permanent magnetization for these alkali/graphite systems. Because our model superstructures do not correspond to the experimental observed phases, this result was not completely unexpected. The magnitudes of the calculated magnetization, however, provide an additional insight about the extent to which the valence electrons of the adatoms retain their atomic-like character. In the case of lithium, we did not observe spin polarization. The majority and minority spin components of the Li-induced states merged into a non-spin-polarized, and empty, band (see Figure 5). On the contrary, the magnetization observed in the Na and K adsorption models indicates that a fraction of the electrons remain in atomic-like states, with this fraction being larger for Na impurities. In fact, for Na and K adatoms the *s*-like alkali-derived electronic states are close to the Fermi level (see Figures 6 and 7). The calculated splittings between the majority and minority spin states were about 0.4 eV for Na and 0.2 eV for K. The most remarkable difference between the dispersion curves shown in Figures 5−7 is the position of the alkali atom induced states. Compared with the graphite's work function, the Na ionization potential (5.1 eV) is larger, whereas potassium's ionization potential (4.34 eV) is slightly lower. Therefore, the occupancy of the localized states might be expected to be larger for Na than for K adatoms;[65] the calculated band structures agreed with that expectation.

In Figure 8, we show the difference electronic charge for Na and K adatoms. Compared with the behavior of the same quantity for Li (Figure 4), there are several remarkable issues. The peak of charge accumulation for the three cases appeared about 0.83 Å above the graphite surface. The width of this feature along the *z* axis, about 1.3 Å measured from the crossing with the zero charge transfer axis, did not change considerably from one adatom to another. Therefore, the charge redistribution in that region might be considered as directly related to the

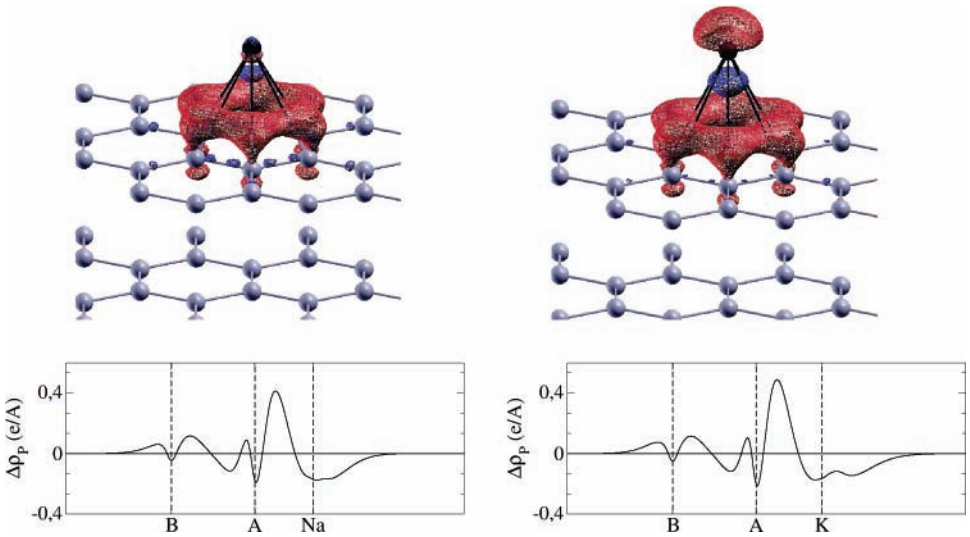

Figure 8. Top: two isosurfaces of the charge density difference, $\Delta\rho = \rho[AC_{64}] - \rho[C_{64}] - \rho[A]$, calculated for the Na/graphite (left panel) and K/graphite (right panel); red surfaces correspond to charge gains of 0.015 e/Å^3 and blue surfaces are for an equivalent charge lost. Bottom: the corresponding difference density integrated over planes lying parallel to the graphite's surface, $\Delta\rho_P = \int_{x,y} \Delta\rho \, dA_\perp$. Only the results from PBE calculations are shown; LSDA gave a very similar picture.

TABLE 5: Estimations of the Charge Transfer in the A/Graphite Systems, A = Li, Na, K[a]

	Δc_B[b]	Δc_{nb}[c]	Δc_1[d]	VDD[e]	Δc_L[f]	D_z (D)[g]
			Li			
LSDA[h]	1.00	0.38 (0.38)	0.38	0.42	0.60 (0.60)	4.97 (4.47)
PBE[h]	0.89	0.38	0.39	0.47		5.43
B3LYP[i]					0.43	
			Na			
LSDA[h]	0.79	0.26 (0.23)	0.35 (0.30)	0.54	0.91	5.56 (4.28)
PBE[h]	0.73	0.28	0.36	0.59		5.64
B3LYP[i]					0.62	
			K			
LSDA[h]	0.84	0.35 (0.28)	0.46 (0.39)	0.70	0.93	8.22 (5.83)
PBE[h]	0.81	0.33	0.46	0.79		8.09
B3LYP[i]					0.84	
LDA[j]			0.38			
LDA[k]			0.40			

[a] We also report some values available in the literature. Values for charge transfer are given in terms of the charge e of the electron. [b] Value estimated from Bader analysis. [c] Change in the charge in the nonbonded region of the alkali atom (eq 3). [d] Charge lost in the negative peaks near the alkali adatoms (eq 4). [e] Voronoy's deformation charge. [f] Charge transfer according to the Löwdin charge analysis. [g] Electric dipole moment in the z direction. [h] This work, using $c_0 = 23.5$ Å; when available, we report also the value obtained by extrapolation (values in parentheses). [i] Mulliken analysis on a cluster model, ref 34. [j] Supercell model with the same adatom's density, ref 22. [k] Supercell model with the same adatom's density, ref 54.

substrate electronic states. There is a significant loss of electronic density in the graphene layer below the alkali atom, and particularly in the closest hexagonal ring, suggesting a reduction in the sp^2 contributions. This feature appeared more dramatically for Li than for the Na and K adatoms. The shape of the electron gain clouds for Li differs from those for Na and K. In these last two cases, we did not observe the significant distortion witnessed for Li.

Our observations regarding the electronic states dispersion curves, and difference electronic charge, suggest that Li adatoms donate more charge to the substrate than the other two studied species, especially compared with Na atoms. Further, they hint at a larger polarization of the substrate electronic cloud by the lithium atoms. In Table 5, we summarize our results for the charge distribution descriptors mentioned in section 3, along with some other quantifications of the charge transfer available in the literature.

The descriptors derived from the charge density difference profiles showed a $\Delta c + \text{constant}/c_0^3$ dependency with the size of the vacuum region; this dependency is related to the induced dipole moment, hence it is more important for the analysis of K adatoms. The values of Δc_{nb} and Δc_1 evidenced the same trend. Löwdin, or Mulliken,[34] charges hint at lower charge transfer for Li. The intrinsic flaws of these two methods, in particular their dependency on the considered projectors/basis sets, compromise their reliability. The dispersion of data in Table 5 must be considered a consequence of the different definitions, each one targeted to different instances of the same phenomena, as discussed in section 3. The same statement holds true for the experimental determination of the charge transfer (see, for example, Table 4 in ref 8). The results from Bader's analysis agreed with the band structure information yielding large values for the charge transfer, with a difference between 0.16 and 0.21 e between the charge donated by Li and Na atoms. The fact that this measure of the charge transfer is smaller for Na, larger for K, and the largest for Li agrees with the respective ionization potentials. If such large fractions of the valence electrons migrate to substrate states, then the electronic charge surrounding the core of the alkali atom could be expected to decrease with the binding distance. The large transfer from adsorbate atomic-like states to the substrate states in Li is compensated by the large density of substrate states at the binding distance, and therefore, a relatively small change of the charge in the Voronoy volume is expected. For potassium, the screening is less efficient due to the larger binding distance and the charge in the Voronoy volume can be expected to be large. In the case of sodium, an intermediate condition holds because relatively less charge is transferred from atomic-like states but the screening is also reduced when compared with the case of Li. This trend in the Voronoy deformation charges was observed.

Therefore, the results for Li, Na, and K indicate a similar binding mechanism: a strong, noncovalent interaction between the substrate's π-electrons and the ionized atom. The differences between them could be understood from their ionic radius and ionization potentials. The small Li radius, and consequent small binding distance, favors the polarization of the π-cloud, thus allowing for an enhanced induction contribution to the binding

energy.[63] The induction energy decays roughly as one over the binding distance to the fourth power,[63] therefore its importance in the Na, and K cases is progressively reduced and the cation$-\pi$ interaction is dominated by purely electrostatic contributions. If we estimate the contribution of the cation$-\pi$ interaction in Na/graphite and K/graphite, from the binding energies in the associated $A^+-C_6H_6$ (A = K, Na) complexes,[61,63] then the binding energies could be expected to be roughly given by

$$E_b(\mathrm{Na}) \sim 0.92\ \mathrm{eV} - (\mathrm{IP[Na]} - W_f[\mathrm{Graphite}]) = 0.42\ \mathrm{eV}$$

and

$$E_b(\mathrm{K}) \sim 0.74\ \mathrm{eV} - (\mathrm{IP[K]} - W_f[\mathrm{Graphite}]) = 1.0\ \mathrm{eV}$$

indicating that the ordering of the binding energies is due to an interplay between the cation$-\pi$ interaction and the energetic cost of charge transfer. Moreover, the larger ionization potential of Na would hinder complete charge transfer.

5. Conclusions

We studied the binding mechanism for Li atoms adsorbed on graphite and compared this case with Na and K adatoms. For this purpose, we used density functional calculations with a slag

geometry, using both the LSDA and PBE approximations to the exchange-correlation energy functional. Although these systems have been already studied in the literature, only one comparative theoretical study[29,34] has been reported to the best of our knowledge. In agreement with their results, we found that the binding energy is larger for K than for Na on graphite. The explanation, reported in that paper, of this particular ordering of the binding energies is based on the existence of HOMO$-$LUMO gaps in the substrate model. Our results favors instead the idea that the binding processes are related to the cation$-\pi$ interaction, which describes the interaction between the corresponding ionized atoms and aromatic rings. Considering the energetic costs associated with the charge transfer, the corresponding binding energies could be expected to be $\sim$1.32 eV (Li), $\sim$0.49 eV (Na), and $\sim$1.0 eV (K). The predictive character of these values, however, should not be overemphasized. In fact, we did not attempt to evaluate the contributions of cation$-\pi$ interactions in the corresponding alkali-cation/graphite systems. However, the above-mentioned estimations correlate accurately to the values given by our DFT calculations, suggesting that this simple interpretation captures the main aspects of the binding mechanisms. The calculated charge distribution profiles appear also to be consistent with the associated cation$-\pi$ complexes, with a significant polarization of the π-cloud for Li adatoms. The statement of this picture, however, depends strongly on whether the electronic charge in the bonding region should be considered to correspond to electrons in proper substrate electronic states. Descriptions of the charge transfer based on quantum mechanical concepts, like Bader's analysis, the electronic band structures, and the position of the maximally localized Wannier functions centers, support this assumption. The delocalized character of these substrate states and polarization effects allows for partial screening of the resulting ions, as can be inferred from simple geometrical partitions of the charge distribution (v.gr., the Voronoy polyhedra and the charge in the nonbonded region). These mechanisms are particularly relevant for lithium adatoms, because of the shorter binding distance.

According to our test calculations on the $Li-C_6H_6$ system, the binding energy was underestimated using the PBE approximation and overestimated in the LSDA framework. This could be also the case for the Li/graphite calculations. Therefore, the values given by our DFT calculations might be considered lower (PBE value, 1.1 eV) and higher (LSDA value, 1.75 eV) bounds. The binding energy is expected to be near the above-mentioned 1.32 eV value, estimated from the cation$-\pi$ interaction and consistent with previously reported cluster calculations using models of the substrate with open electronic shell states.

We believe that these estimations and the description of the binding mechanism represent a significant advance in the understanding of Li adsorption on graphite. Moreover, our study of the dependence of the binding energy with the considered calculation parameters helps to rationalize the dispersion in the previously reported data and provide important hints for further investigations. We have shown that a proper description of the substrate electronic band structure, especially near the Fermi level, is required to obtain meaningful results. In particular, if the models used for the substrate have significant electronic gaps, as is the case for cluster models with closed-shell electronic states and slabs calculations using only the Γ-point to sample the Brillouin zone, then the binding energies are expected to be largely underestimated. We have also shown that inclusion of a second graphene layer affects the calculated binding energy, increasing it by about 0.1 eV. A very precise, that is, with chemical accuracy, evaluation of the binding energy of this system is still hindered by several technical difficulties. The interaction between neighboring adatoms in supercell calculations might give rise to important underestimations, unless huge supercell sizes are used. Moreover, correlation effects, which are not entirely taken into account by our approach, are relevant in Li$-$aromatic and Li^+-aromatic complexes,[59] and they could also play an important role in the Li/graphite system.

Acknowledgment. We acknowledge funding from Padua University Project No. CPDA033545 and PRIN 2004 ("NANOTRIBOLOGIA" project) and allocation of computer resources from INFM "*Progetto Calcolo Parallelo*". A.H.R. acknowledges support from CONACYT-Mexico through Grant J-42647-F.

References and Notes

(1) Jungblut, B.; Hoinkis, E. *Phys. Rev. B* **1989**, *40*, 10810.
(2) Hu, Z. P.; Ignative, A. *Phys. Rev. B* **1984**, *30*, 4856.
(3) Dresselhaus, M. S.; Dresselhaus, G. *Adv. Phys.* **1981** *30*, 139.
(4) Woo, K. C.; Mertwoy, H.; Fischer, J. E.; Kamitakahara, W. A.; Robinson D. S. *Phys. Rev. B* **1983**, *27*, 7831.
(5) Di Vincenzo, D. P.; Mele, E. J. *Phys. Rev. Lett.* **1984**, *53*, 52.
(6) Nagaura, T. *Prog. Batteries Sol. Cells* **1990**, *9*, 209.
(7) Tarascon, J.-M.; Armand, M. *Nature* **2001**, *414*, 359.
(8) Caragiu, M.; Finberg, S. *J. Phys: Condens. Matter* **2004**, *17*, R995.
(9) Pivetta, M.; Patthey, F.; Barke, I.; Hövel, H.; Delley, B.; Schneider, W.-D. *Phys. Rev. B* **2005**, *71*, 165430.
(10) Ferralis, N.; Pussi, K.; Finberg, S. E.; Smerdon, J.; Lindroos, M.; Mc. Grath, R.; Diehl, R. D. *Phys. Rev. B* **2004**, *70*, 245407.
(11) Kahntha, M.; Cordero, N. A.; Molina, L. M.; Alonso, J. A.; Grifalco, L. A. *Phys. Rev. B* **2004**, *70*, 125422.
(12) Rytknönen, K.; Akola, J.; Manninen, M. *Phys. Rev. B* **2004**, *69*, 205404.
(13) Breitholtz, M.; Kihlgren, T.; Lindgren, S.-Å; Walldén, L. *Phys. Rev. B* **2003**, *67*, 235416.
(14) Breitholtz, M.; Kihlgren, T.; Lindgren, S.-Å; Walldén, L. *Phys. Rev. B* **2002**, *66*, 153401.
(15) Lou, L.; Österlund, L.; Hellsing, B. *J. Chem. Phys.* **2000**, *112*, 4788.
(16) Bennich, P.; Puglia, C.; Brühwiler, P. A.; Nilsson, A.; Maxwell, A. J.; Sandell, A.; Märtensson, N.; Rudolf, P. *Phys. Rev. B* **1999**, *59*, 8292.
(17) Sandell, A.; Brühwiler, P. A.; Nilsson, A.; Bennich, P.; Rudolf, P.; Märtensson, N. *Surf. Sci.* **1999**, *429*, 309.

(18) Hjorstam, O.; Wills, J. M.; Johansson, B.; Eriksson, O. *Phys. Rev. B* **1998**, *58*, 13191.
(19) Österlund, L.; Chakarov, D. V.; Kasemo, B. *Surf. Sci.* **1999**, *420*, 174.
(20) Sandell, A.; Hjorstam, O.; Nilsson, A.; Brühwiler, P. A.; Eriksson, O.; Bennich, P.; Rudolf, P.; Wills, J. M.; Johansson, B.; Märtensson, N. *Phys. Rev. Lett.* **1997**, *78*, 4994.
(21) Hock, K. M.; Barnard, J. C.; Palmer, R. E.; Ishida, H. *Phys. Rev. Lett.* **1993**, *71*, 641.
(22) Ancilotto, F.; Toigo, F. *Phys. Rev. B* **1993**, *47*, 13713.
(23) Janiak, C.; Hoffmann, R.; Sjövall, P.; Kasemo, B. *Langmuir* **1993**, *9*, 3427.
(24) Ishida, H.; Palmer, R. E. *Phys. Rev. B* **1992**, *46*, 15484.
(25) Li, Z. Y.; Hock, K. M.; Palmer, R. E. *Phys. Rev. Lett.* **1991**, *67*, 1562.
(26) Wu, N. J.; Ignatiev, A. *Phys. Rev. B* **1983**, *28*, 7288.
(27) Cabria, I.; Lopez, M. J.; Alonso, J. A. *J. Chem. Phys.* **2005**, *123*, 204721.
(28) White, J. D.; Cui, J.; Strauss, M.; Diehl, R. D.; Ancilotto, F.; Toigo, F. *Surf. Sci.* **1994**, *307*−*309* 1134.
(29) Zhu, Z. H.; Lu, G. Q.; Wang F. Y. *J. Phys. Chem. B* **2005**, *109*, 7923.
(30) Kurita, N. *Carbon* **2000**, *38*, 65.
(31) Dubot, P.; Cenedese, P. *Phys. Rev. B* **20001**, *63*, 241402.
(32) Shimizu, A.; Tachikawa, H. *J. Phys. Chem. Solids* **2003**, *64*, 807.
(33) Constance, B. E. F.; Rao, B. K. In *Clusters and nano-assemblies: Physical and Biological systems*, Proceedings of the International Symposium, Richmond, VA, Nov. 10−13, 2003; Jena, P., Khanna, S. N., Rao B. K., Eds.; World Scientific Publishing Co.: Singapore, 2005.
(34) Zhu, Z. H.; Lu, G. Q. *Langmuir* **2004**, *20*, 10751.
(35) Zhao, J.; Buldum, A.; Han, J.; Lu, J. P. *Phys. Rev. Lett.* **2000**, *85*, 1706.
(36) Meunier, V.; Kephart, J.; Roland, C.; Bernholc, J. *Phys. Rev. Lett.* **2002**, *88*, 075506.
(37) Nishidate, K.; Hasegawa, M. *Phys. Rev. B* **2005**, *71*, 245418.
(38) Perdew, J. P.; Zunger, A. *Phys. Rev. B* **1981**, *23*, 5048.
(39) Perdew, J. P.; Burke, K.; Ernzerhof, M. *Phys. Rev. Lett.* **1996**, *77*, 3865.
(40) von Barth, U.; Pedroza, A. C. *Phys. Scripta* **1985**, *32*, 353.
(41) Louie, S. G.; Froyen, S.; Cohen, M. L. *Phys. Rev. B* **1982**, *26*, 1738.
(42) Andreoni, W.; P. Giannozzi, P.; Parrinello, M. *Phys. Rev. Lett.* **1994**, *72*, 848.
(43) Andreoni, W.; Giannozzi, P.; Parrinello, M. *Phys. Rev. B* **1995**, *51*, 2087.
(44) Andreoni, W.; Giannozzi, P.; Armbruster, J. F.; Knupfer, M.; Fink, J. *Europhys. Lett.* **1996**, *34*, 699.
(45) Vanderbilt, D. *Phys. Rev. B* **1990**, *41* (Rapid Communication), 7892.
(46) The C, Li, and Na pseudopotentials were taken from the pwscf pseudopotential library: http://www.pwscf.org/pseudo.htm. The carbon pseudopotential was generated by Bernd Meyer 2002; Li and Na pseudopotentials were generated by Axel Kohlmeyer (2005 and 2006).
(47) Baroni, S.; Dal Corso, A.; de Gironcoli, S.; Giannozzi, P.; Cavazzoni, C.; Ballabio, G.; Scandolo, S.; Chiarotti, G.; Focher, P.; Pasquarello, A.; Laasonen, K.; Trave, A.; Car, R.; Marzari, N.; Kokalj, A. http://www.pwscf.org/.
(48) Jansen, H. J. F.; Freeman, A. J. *Phys. Rev. B* **1987**, *35*, 8207.
(49) Trickey, S. B.; Müller-Plathe, F.; Diercksen, G. H. F.; Boettger, J. C. *Phys. Rev. B* **1992**, *45*, 4460.
(50) Dunlap, B. I.; Boettger, J. C. *J. Phys. B: At., Mol. Opt. Phys.* **1996**, *29*, 4907.
(51) Boettger, J. C. *Phys. Rev. B* **1997**, *55*, 11202.
(52) Hasegawa, M.; Nishidate, K. *Phys. Rev. B* **2004**, *70*, 205431.
(53) Birch, F. *Phys. Rev.* **1947**, *71*, 809.
(54) Lamoen, D.; Persson, B. N. J. *J. Chem. Phys.* **1998**, *108*, 3332.
(55) Shanno, D. F. *Math. Comput.* **1970**, *24*, 647.
(56) Bader, R. *Atoms in Molecules: A Quantum Theory*; Oxford University Press: New York, 1990.
(57) Bader, R.; Henneker, W. H.; Cade, P. E. *J. Chem. Phys.* **1967**, *46*, 3341.
(58) Guerra, F. C.; Handgraaf, J. W.; Baerends, E. J.; Bickelhaupt, F. M. *J. Comput. Chem.* **2004**, *30*, 189.
(59) Vollmer, J. M.; Kandalam, A. K.; Curtis, L. A. *J. Phys. Chem. A* **2002**, *106*, 9533.
(60) We used the method developed by Henkelman, G.; Arnaldsson, A.; Jonsson, H. *Comput. Mater. Sci.* **2006**, in press.
(61) Ma, J. C.; Dougherty, D. *Chem. Rev.* **1997**, *97*, 1303.
(62) Marzari, N.; Vanderbilt D. *Phys. Rev. B* **1997**, *56*, 12847.
(63) Tsuzuki, S.; Yoshida, M.; Uchimaru, T.; Mikami, M. *J. Phys. Chem. A* **2001**, *105*, 769.
(64) Gal, J.-F.; Maria, P.-C.; Decouzon, M.; Mó, O.; Yañez, M.; Abboud, J. L. M. *J. Am. Chem. Soc.* **2003**, *125*, 10394.
(65) Gurney, R. W. *Phys. Rev.* **1935**, *47*, 479.
(66) Reich, S.; Thomsen, C.; Ordejón, P. *Phys. Rev. B* **2002**, *65*, 153407.